Cooperative Eco-Driving of Electric Vehicle Platoons for Energy Efficiency and String Stability

Vinith Kumar Lakshmanan, Antonio Sciarretta, Ouafae El Ganaoui-Mourlan

Available online at www.sciencedirect.com

ScienceDirect

IFAC PapersOnLine 54-2 (2021) 133–139

Cooperative Eco-Driving of Electric Vehicle Platoons for Energy Efficiency and String Stability

Vinith Kumar Lakshmanan * **Antonio Sciarretta** **
Ouafae El Ganaoui-Mourlan ***

* *IFP Energies Nouvelles, Rueil-Malmaison, France (e-mail: name-middlename.surname@ifpen.fr)*
** *IFP Energies Nouvelles, Rueil-Malmaison, France (e-mail: name.surname@ifpen.fr)*
*** *IFP School, Rueil-Malmaison, France (e-mail: name.surname@ifpen.fr)*

Abstract: This paper discusses cooperation applied to a platoon of electric vehicles using an Eco-Driving Optimal Controller (EDOC). The proposed algorithm is evaluated in terms of energy efficiency and string compactness in comparison with the non-cooperative EDOC and standard adaptive cruise control using a drive cycle based scenario. A theoretical analysis of string stability with and without cooperation is presented. The simulation results show that a platoon with cooperative EDOC performs better in terms of energy efficiency and string compactness than without cooperation.

Keywords: Eco-driving, cooperation, nonlinear and optimal control

1. INTRODUCTION

Energy consumption related to transport and air quality issues continue to attract the attention of scientists. Various emerging technologies have been proposed and/or developed to address these issues. Even with electric vehicles, which reduce local CO_2 and pollutant emissions with respect to fuel-powered vehicles, overcoming barriers such as range anxiety and increase acceptance by the public requires new energy-efficiency measures.

The adoption of an energy-efficient driving style is the goal of eco-driving techniques. Studies such as Araque et al. (2018); Qi et al. (2017) have demonstrated the energy benefits of using such techniques. In the last decade, eco-driving has been formulated as an optimal control problem, where the vehicle speed is controlled (either directly or indirectly advising the driver) to minimize its energy consumption in a certain horizon, see Sciarretta and Vahidi (2020); Han et al. (2018); Shen et al. (2020); Mahler and Vahidi (2014); Wang et al. (2014); Maamria et al. (2016).

Several driving scenarios can be the object of eco-driving. One such scenario (car following) involves two or more vehicles following closely with each other, where each vehicle must maintain a safe minimum gap with respect to the preceding one. Such vehicular platoons (or "strings") can suffer from string instability, where the spacing gaps amplify along the string.

To study the dynamics of vehicular platoons, some relevant characteristics must be considered. In terms of composition, a platoon can be homogeneous or heterogeneous. A homogeneous platoon assumes same dynamics for all the vehicles; its string stability properties have been studied in Peppard (1974); Xiao and Gao (2011); Swaroop and Hedrick (1999); Seiler et al. (2004); Swaroop and Hedrick (1996). A heterogeneous platoon, on the other hand, assumes that vehicles in the platoon can have different dynamics, see Shaw and Hedrick (2007); Naus et al. (2010); Sheikholeslam and Desoer (1990).

Secondly, the car following control law assumed to be used by the vehicles in the platoon must be considered. Extensive literature exits on string stability of platoons using Adaptive Cruise Control (ACC). With ACC the control law is based only on the on-board sensors, such as radar, lidar or a camera setup, which measure the relative speed and distance with the preceding vehicle that is then fed as input to the controller. Then the acceleration is determined in order to follow a desired spacing policy. With a constant spacing policy, a constant safe distance is tracked, see Swaroop and Hedrick (1999); Peppard (1974). With a constant-time headway policy the desired gap is velocity-dependent, see Naus et al. (2010); Xiao and Gao (2011). Nonlinear spacing policies have been also proposed, see Yanakiev and Kanellakopoulos (1998). Studies such as Swaroop and Hedrick (1999); Naus et al. (2010); Seiler et al. (2004) have shown that ACC with a constant spacing strategy exhibits string instability, whose mitigation requires to adopt a constant-time headway policy with a certain minimum headway time Naus et al. (2010); Xiao and Gao (2011).

Thirdly, vehicles in the platoon can be also assumed to communicate amongst each other using wireless V2V technology. ACC with the additional functionality to communicate with the preceding vehicle to receive its current

10.1016/j.ifacol.2021.06.018

acceleration is called as Cooperative Adaptive Cruise Control (CACC). Rajamani and Chunyu Zhu (1999); Naus et al. (2010) have shown that a CACC platoon can be string stable using a constant headway policy but with a smaller minimum headway time compared to an ACC using the same policy.

On the other hand, Dollar et al. (2020) have described the use of a non-cooperative Eco-Driving Optimal Controller (EDOC) [1] in a platoon. The authors assessed the energy efficiency and string compactness of this algorithm in comparison to a standard ACC scheme as a baseline. Their study showed that the EDOC saves energy for the first followers but is string unstable and thus displays larger overall energy consumption for strings of several vehicles. Consequently, more complex eco-driving hierarchical schemes are necessary to improve both aspects.

The drawbacks of the EDOC in the car following scenario demonstrated by Dollar et al. (2020) is taken as motivation for this study. The goals of this paper are to explore if cooperation can help improve energy efficiency and string stability in a platoon and analyze under which conditions instabilities occur. Cooperation is introduced in the platoon as the ability to share the intentions over a certain horizon, see Dunbar and Murray (2006). We assume that each vehicle shares the result of its own eco-driving optimization, i.e., its intended accelerations over the near future, with its following vehicle. We thus use the term cooperation differently as with CACC, where only the current acceleration is shared.

This paper is organized as follows. Section 2 introduces the longitudinal vehicle model and a description of the platoon. In Section 3, we review the electric vehicle eco-driving optimal controller and its implementation. We also introduce the concept of cooperation. Section 4 presents the string stability analysis of the various control inputs. Finally, Section 5 shows the simulation results on energy consumption and string stability.

2. VEHICLE AND PLATOON MODEL

In this section we describe the vehicle model and the characteristics of the vehicular platoon controlled by EDOC.

2.1 Vehicle Model

The longitudinal motion of the vehicle is captured by a simple model given by Newton's second law,

$$\begin{aligned} m\dot{v} &= F_t - (F_a + F_r + F_g) - F_b \\ &= F_t - \frac{1}{2}\rho_a c_d A_f v^2 - mgc_r - mg\sin(\alpha(s)) - F_b \,, \end{aligned} \tag{1}$$

where F_t, F_a, F_r, F_g, and F_b are the traction force given by the powertrain at the wheels, the aerodynamic resistance, rolling resistance, resistance due to gravity and the mechanical breaking force respectively. The velocity of the vehicle is indicated with v, $a = \dot{v}$ indicates the vehicle acceleration, m is the mass of the vehicle. For the sake of simplicity, the inertial masses are neglected. The parameters that contribute to the aerodynamic drag are ρ_a, c_d, A_f, which denote the external air density, aerodynamic drag coefficient, and vehicle frontal area respectively. The parameters that contribute to the rolling and gravity resistances are c_r, the rolling resistance coefficient, g the gravitational constant, and α, the road slope as a function of the position s.

[1] Referred to as Position-Constrained Shrinking Horizon Control (PCSHC) in that paper.

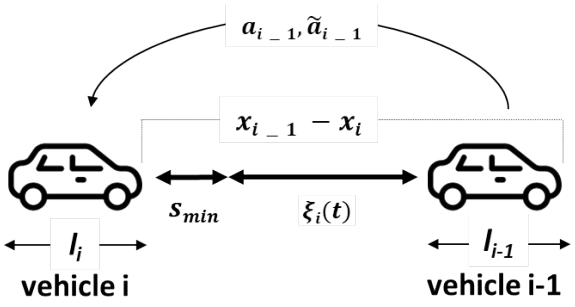

Fig. 1. Illustration of a platoon.

From the power at the wheels $P_t = vF_t$, the energy consumption at the battery P_b is calculated using simple transmission and electric motor models, inspired by those used in Dib et al. (2011),

$$P_b = p_0 P_t + p_1 F_t^2 \,, \tag{2}$$

where p_0 and p_1 are constant model parameters. The battery and power-link losses are neglected in this study.

2.2 Platoon Model

As shown in Fig. 1, the platoon uses predecessor–following communication topology where each vehicle communicates only with the nearest preceding vehicle. All vehicles in the platoon have the same plant dynamics (homogeneous platoon) and use constant spacing policy. In a platoon consisting of $N+1$ vehicles, each vehicle is indexed i from 1 to N. The first vehicle or the leader in the platoon is indexed $i = 0$, which acts as the reference trajectory for the platoon. The index of the vehicles increases going upstream in the platoon. For example, the vehicle preceding the i-th vehicle is denoted as $i-1$ and the vehicle following as $i+1$.

Let $v_i(t)$, $x_i(t)$, l_i denote the speed, position, and the length of the i-th (ego) vehicle, whereas $v_{i-1}(t)$, $x_{i-1}(t)$, and $a_{i-1}(t)$ denote the speed, position, and current acceleration of the preceding vehicle. The control variable of each vehicle is chosen as the net force produced by the powertrain per unit mass, i.e., the acceleration a_i. With these definitions, the longitudinal vehicle model can be rewritten in state-space form as

$$\dot{X}_i(t) = A_i X_i(t) + B_i U_i(t) \,, \tag{3}$$

where

$$\begin{aligned} X_i(t) &= \begin{bmatrix} x_i(t) \\ v_i(t) \end{bmatrix} \,, \quad A_i = \begin{bmatrix} 0 & 1 \\ 0 & 0 \end{bmatrix} \,, \\ B_i &= \begin{bmatrix} 0 \\ 1 \end{bmatrix} \,, \quad U_i(t) = a_i(t) \,. \end{aligned} \tag{4}$$

The spacing error between the vehicles i and $i-1$ is defined as

$$\begin{aligned} \xi_i(t) &= x_{i-1}(t) - x_i(t) - l_{i-1} - s_{i,i-1}(t) \,, \\ \dot{\xi}_i(t) &= v_{i-1}(t) - v_i(t) \,, \end{aligned} \tag{5}$$

where $s_{i,i-1}$ is the minimum safe inter-vehicle distance, which can either be a constant, s_{min} (as in the case of (5)), or resulting from a constant-time headway, $v_i H$.

In a standard ACC, the feedback control law $U_i(v_i, \xi_i, \dot{\xi}_i)$ is given by

$$a_i(t) = k_p \xi_i(t) + k_v \dot{\xi}(t) \ . \tag{6}$$

The main goal of ACC is to follow the preceding vehicle with the desired safe distance. However, we aim at deriving a car following feedback control law, of the form, $U_i(v_i, \xi_i, \dot{\xi}_i, ...)$, such that each vehicle not only follows its predecessor, but does it in an energy-efficient way.

3. ECO-DRIVING OF ELECTRIC VEHICLES

In this section, eco-driving of an electric vehicle is formulated as an optimal control problem with an objective function that represents the battery energy consumption. Following the method in Sciarretta and Vahidi (2020); Han et al. (2018), this problem is solved using Pontryagin's Minimum Principle, eventually yielding the feedback control law sought.

3.1 Unconstrained problem

Generally, the main goal of eco-driving is to minimize the cumulative energy consumed over a trip while guaranteeing vehicle safety. Under the simplifying assumptions that friction brakes are not used and that resistance losses are represented by a constant term h, the corresponding optimal control problem for vehicle i in the absence of a preceding vehicle can be formulated as

$$a_i(t) = \mathbf{arg\ min} \int_0^{T_i} \left[p_0 \left(a_i(t+k) + h \right) v_i(t+k) + p_1 \left(a_i(t+k) + h \right)^2 \right] dk \tag{7}$$

subject to

$$x_i(T_i) = D_i \ , \qquad \dot{x}_i = v_i(t) \ ,$$
$$v_i(T_i) = V_i \ , \qquad \dot{v}_i = a_i(t) \ ,$$

where the running cost is derived from (2), T_i is the optimization horizon, while D_i and V_i are the distance to be covered in the horizon and the desired speed at its end. The solution of (7) yields a parabolic speed profile as a function of time,

$$v_i(t+k) = v_i(t) + \left(-\frac{4v_i(t)}{T_i} - \frac{2V_i}{T_i} + \frac{6D_i}{T_i^2} \right) k + \left(\frac{3v_i(t)}{T_i^2} - \frac{6D_i}{T_i^3} + \frac{3V_i}{T_i^2} \right) k^2, \quad k \in [0, T_i) \ . \tag{8}$$

3.2 Position-constrained problem

In this scenario, the ego vehicle tries to avoid a rear-end collision with the preceding vehicle which imposes state inequality constraint $\xi_i(t+k) \geq 0$, that is,

$$x_i(t+k) \leq x_i(t) + \xi_i(t) + v_{i-1}(t)k + \frac{1}{2} a_{i-1}(t) k^2 \ , \tag{9}$$

where the PV is assumed to keep its acceleration $a_{i-1}(t)$ constant during the whole horizon. In the presence of the constraint (9), the optimal speed profile is calculated as

$$v_i(t+k) = v_i(t) + \left(a_{i-1}(t) + \frac{4}{\theta_i}\dot{\xi}_i(t) + \frac{6}{\theta_i^2}\xi_i(t) \right) k - \left(\frac{6}{\theta_i^3}\xi_i(t) + \frac{3}{\theta_i^2}\dot{\xi}(t) \right) k^2, \quad k \in [0, \theta_i) \ , \tag{10}$$

where θ_i denotes the contact time where the position constraint is met ($\xi_i(\theta_i) = 0$) and is found by solving the cubic equation

$$\left(v_i(t) - V_i + a_{i-1}(t) T_i\right) \theta_i^3 + \left(4v_{i-1}(t)T_i + V_i T_i - 2v_i(t)T_i + \frac{a_{i-1}(t)T_i^2}{2} - 3D_i \right) \theta_i^2 + \left(6\xi_i(t)T_i + v_i(t)T_i^2 - v_{i-1}(t)T_i^2 \right) \theta_i - 3\xi_i(t)T_i^2 = 0 \tag{11}$$

3.3 Feedback control law

Since the speed and the acceleration of the preceding vehicle (PV) are generally varying in time, the solutions of the eco-driving problem derived in the previous sections are embodied in a Model Predictive Control (MPC) paradigm. Accordingly, V_i, D_i, and T_i are updated at each time t, $x_i(t) = 0$, and the control input U_i is evaluated from (8) or (10) and $k = 0$.

Therefore, if the position trajectory of the preceding vehicle does not intersect the unconstrained position trajectory of the ego vehicle, then the eco-driving control input is given by

$$a_i(t) = -\frac{4}{T_i} v_i(t) - \frac{2}{T_i} V_i + \frac{6}{T_i^2} D_i \ . \tag{12}$$

If the position trajectory of the preceding vehicle does intersect with the unconstrained position trajectory of the ego vehicle, then the eco-driving control input is given by

$$a_i(t) = a_{i-1}(t) + \frac{4}{\theta_i}\dot{\xi}_i(t) + \frac{6}{\theta_i^2}\xi_i(t) \ . \tag{13}$$

The control law (13) is structurally similar to that of ACC, however, it also depends on the acceleration of the PV.

Note that we have omitted the time dependency from the horizon and the terminal conditions, as if they were constant (receding horizon paradigm). However, the same consideration apply when these quantities continuously change in time (shrinking horizon paradigm).

The assumption of a constant acceleration for the preceding vehicle could render the controllers (12)–(13) infeasible in certain situations. For instance, when PV acceleration a_{i-1} is negative, it is possible that PV stops at a time $t_{stop} = v_{i-1}/|a_{i-1}| < T_i$ hindering the ego vehicle from reaching its final position D_i. In this situation the boundary conditions of the ego vehicle are updated to that of the preceding vehicle,

$$V_i = 0 \ , \qquad D_i = \xi_i(t) + \frac{v_{i-1}(t)^2}{2|a_{i-1}(t)|} \ . \tag{14}$$

Substituting these boundary conditions in (12), the control input is modified as

$$a_i(t) = -\frac{4}{T_i} v_i(t) + \frac{6}{T_i^2}\xi_i(t) + \frac{3}{T_i^2}\frac{v_{i-1}(t)^2}{a_{i-1}(t)} \ . \tag{15}$$

Another scenario that could render (12)–(13) infeasible during PV deceleration, is when it stops at a time $t_{stop} >$

T_i but at a position lower than D_i. The updated boundary conditions are therefore given by:

$$V_i = v_{i-1}(t) + a_{i-1}(t)T_i \ ,$$
$$D_i = x_{i-1}(T_i) = \xi_i(t) + v_{i-1}(t)T_i + \frac{a_{i-1}(t)T_i^2}{2} \ . \quad (16)$$

Substituting these boundary conditions in (12), the control input is obtained as

$$a_i(t) = a_{i-1}(t) + \frac{4}{T_i}\dot{\xi}_i(t) + \frac{6}{T_i^2}\xi_i(t) \ . \quad (17)$$

3.4 Cooperation-intention sharing

Cooperation is introduced in the platoon as the ability to share the intentions over a certain horizon. Each vehicle in a platoon solves its own OCP and sends its solution to the following vehicle. In order to be used in the eco-driving control of the ego vehicle, this information is lumped into one "future mean value" $\tilde{a}_{i-1}$, evaluated over a preview window length L, as

$$\tilde{a}_{i-1}(t) = \frac{1}{L}\int_t^{t+L} a_{i-1}(\tau)d\tau \ . \quad (18)$$

This future mean PV acceleration $\tilde{a}_{i-1}(t)$ replaces the measured acceleration $a_{i-1}(t)$ in all equations of the previous section.

4. STRING STABILITY ANALYSIS

In this section we analyse if the various control inputs mentioned in section 3.3, in particular (13), (17), (15), are string stable. We assume that the eco-driving controller uses constant spacing policy. As mentioned in the introduction, string stability implies that the spacing errors are attenuated as we go upstream in a platoon. A frequency-domain string stability definition proposed in Swaroop and Hedrick (1996) is used in this analysis, where the error dynamics is given by

$$\ddot{\xi}_i(t) = a_{i-1}(t) - a_i(t) \ . \quad (19)$$

The condition for string stability is given as

$$|G_i(j\omega)| = \left|\frac{\xi_i(j\omega)}{\xi_{i-1}(j\omega)}\right| \leq 1 \ , \forall \ \omega > 0, \quad (20)$$

while $|G_i(j\omega)| = 1, \ \forall \ \omega > 0$ is denoted as marginal string stability. $j\omega$ is replaced with s in following transfer functions for readability. The limitation of the proposed condition for string stability is that it applies only to linear time invariant system. Feedback laws (13), (17) resemble that of a CACC, if we consider θ_i and T_i as constants and $6/\{\theta_i^2, T_i^2\}$, $4/\{\theta_i, T_i\}$ to represent the proportional and the derivative gains of ξ_i and $\dot{\xi}_i$, respectively. However, under a shrinking horizon MPC scheme, these gains evaluated at each time t change depending on the boundary conditions. Thus we considered a receding horizon implementation where the gains $6/T_i^2, 4/T_i^2$ remain constant and an average θ_i over one such cycle is used such that also $6/\theta_i^2, 4/\theta_i$ remain constant.

In doing so, (13), (17) can be written as

$$a_i = a_{i-1} + k_p\xi_i + k_v\dot{\xi}_i \quad (21)$$

where

$$k_p = \frac{6}{T_i^2} \text{ or } k_p = \frac{6}{\theta_i^2}$$
$$k_v = \frac{4}{T_i} \text{ or } k_v = \frac{4}{\theta_i}$$

Taking Laplace transform of (21) we obtain the string stability transfer function

$$|G_i(s)| = \left|\frac{\xi_i}{\xi_{i-1}}\right| = \left|\frac{s^2 + k_v s + k_p}{s^2 + k_v s + k_p}\right| = 1 \ , \ \forall \ \omega > 0 \quad (22)$$

Hence, in this case only marginal string stability $|G_i(s)| = 1 \ , \ \forall \ \omega > 0$ can be guaranteed. The magnitude on a Bode plot would be a straight line at 0 dB for all frequencies $\omega > 0$. Control input (15) is however non-linear in v_{i-1} and a_{i-1}. It is therefore linearized near an equilibrium point to obtain its string stability transfer function.

$$|G_i(s)| = \left|\frac{\xi_i}{\xi_{i-1}}\right| = \left|\frac{k_{ap}s^2 + k_{vp}s + k_{sp}}{s^2 - k_v s + k_{sp}}\right| \quad (23)$$

with

$$k_v = -\frac{4}{T_i} \qquad k_{sp} = \frac{6}{T_i^2}$$
$$k_{vp} = \frac{6v_{i-1}}{a_{i-1}T_i^2} \quad k_{ap} = -\frac{3v_{i-1}^2}{a_{i-1}^2 T_i^2}$$

Using, e.g., $v_{i-1} = v_i$, $a_{i-1} = 0.01$ m/s^2 and T_i= 630 s, the magnitude of the transfer function of (23), $|G_i(s)| > 1$, at small frequencies indicating string instability.

4.1 With Cooperation

Applying the idea of cooperation introduced in (18), where a_{i-1} is replaced by $\tilde{a}_{i-1}$, (21) can be rewritten as:

$$a_i = \tilde{a}_{i-1} + k_p\xi_{i-1} + k_v\dot{\xi}_i \quad (24)$$

where

$$\tilde{a}_{i-1} = \frac{1}{L}\int_t^{t+L} a_{i-1}(\tau)d\tau$$

Taking Laplace transform of (24) yields the transfer function,

$$|G_i(s)_{coop}| = \left|\frac{\xi_i}{\xi_{i-1}}\right| = \left|\frac{\left(k_v + \frac{(e^{sL}-1)}{L}\right)s + k_p}{s^2 + k_v s + k_p}\right| \quad (25)$$

with $|G_i(s)_{coop}|$ is solved numerically to analyse the Bode magnitude plot. Figure 2 shows the Bode magnitude plot of the transfer function $|G_i(s)_{coop}|$ of (25) with $T_i = 630$ and with varying preview window length L. It can be observed that $|G_i(s)_{coop}| < 1, \ \forall \ \omega > 0$, indicating string stability. Similarly using $\tilde{a}_{i-1}$ in the linearised form of (15), leads to the transfer function,

$$|G_i(s)_{coop}| = \left|\frac{\xi_i}{\xi_{i-1}}\right| = \left|\frac{\left(k_{vp} + k_{ap}\frac{(e^{sL}-1)}{L}\right)s + k_{sp}}{s^2 - k_v s + k_p}\right| \quad (26)$$

However the magnitude of the above transfer function is not always less than 1 and requires a more in-depth analysis to determine the conditions for string stability.

5. SIMULATION RESULTS

This section discusses the simulation results of energy assessment and mean string length. Three decentralized

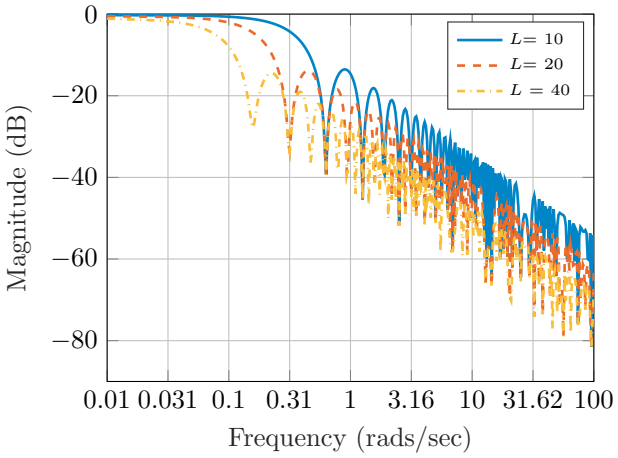

Fig. 2. Bode Magnitude Plot of transfer function (25)

homogeneous platoons, each with $N = 5$, with different algorithms are simulated. The first one is equipped with an ACC using a constant headway time of 1.2 s. The second platoon, is equipped with non-cooperative eco-driving and the third platoon equipped with cooperative eco-driving. The WLTC High drive cycle is used for energy assessment and the string compactness is assessed using the mean string length. The leader in the platoon $i = 0$, acting as the virtual reference trajectory, follows the WLTC cycle in open loop covering a fixed distance D_i in a fixed time T_i. The energy saving of platooning, due to reduced aerodynamic drag, though significant in heavy duty trucks, is assumed to be negligible for passenger electric vehicles and is not highlighted in this study.

5.1 Energy Analysis

Non-Cooperative Eco-Driving with a single follower consumes 4.37 MJ while an ACC consumes 4.41 MJ over a WLTC High cycle. As mentioned in the introduction, Dollar et al. (2020) showed that, non-cooperative eco-driving saves energy for the first follower but it is string unstable and displays larger overall energy consumption as a platoon. Figure 3 shows a comparison between the platoon energy consumption and the mean string length excluding the virtual reference vehicle $i = 0$. Eco-driving with cooperation having $L = 22$ s performs better in terms of energy consumed and does so with a much more compact string on average in comparison with the other platoons.

Figure 4 shows the velocity trajectories of the three different platoons with the different controllers. It can be seen that, eco-driving without cooperation, using a_{i-1} smoothens out certain speed fluctuations of the reference trajectory but appears to have certain discontinuities (sharp decelerations), when the leader is decelerating aggressively (for example between 50 s and 100 s). On the other hand, the velocity trajectories of the eco-driving with cooperation, using $\tilde{a}_{i-1}$ has reduced discontinuities and follows a much smoother trajectory. The cause of these sharp decelerations is explained in much more detail in the following subsection in a better controlled environment.

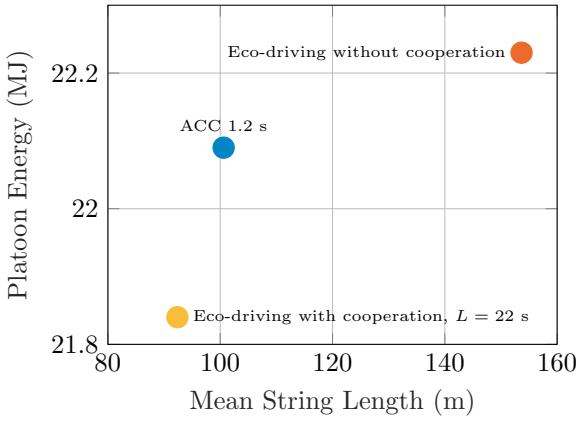

Fig. 3. Platoon Energy and mean string length in WLTC High Cycle

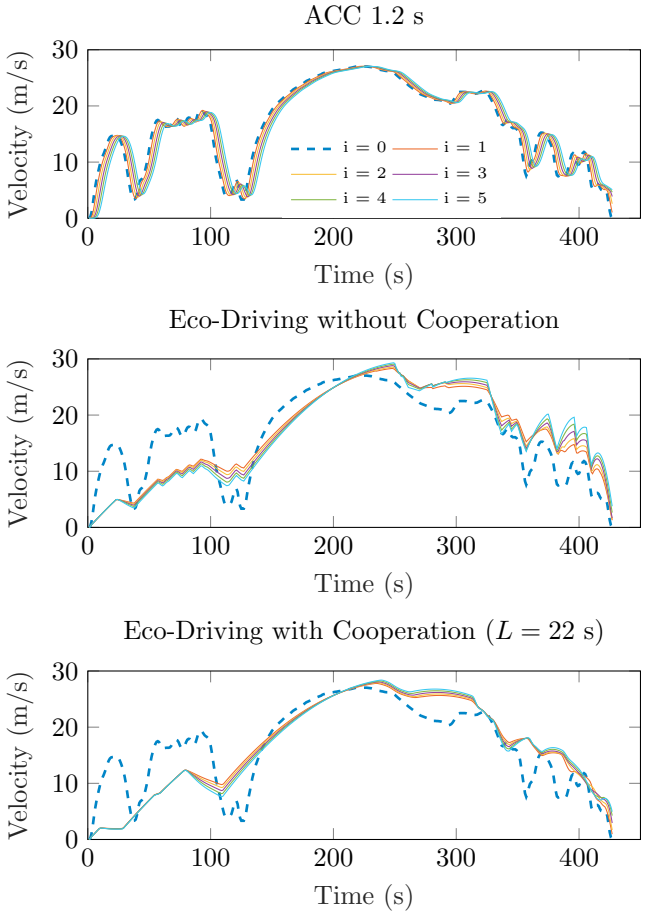

Fig. 4. Velocity Trajectories in the WLTC High Cycle

5.2 Specific Case Study

In this subsection we detail the discontinuities observed in the velocity trajectories of eco-driving without cooperation in Figure 4. The situation simulated here shows a decentralized homogeneous platoon with $N = 10$ under a sinusoidal perturbation of frequency $\omega = 0.01$ rads/s and final time $T_i = 630$ s. The vehicles in a platoon start with the same initial velocity and a certain initial separation greater than s_{min}.

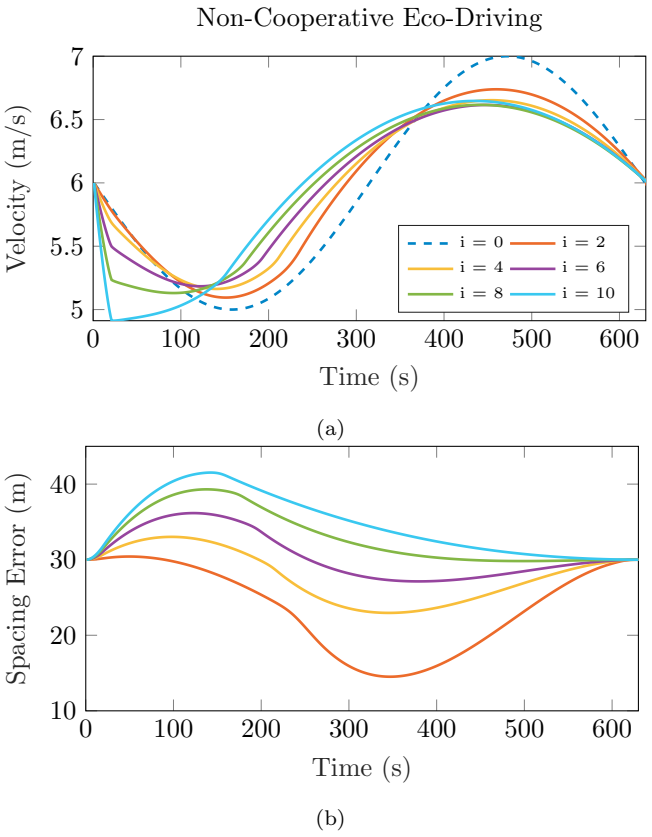

Fig. 5. Velocity profile and spacing error of an eco-driving platoon ($N = 10$) under a sinusoidal perturbation of the leader, without cooperation (a, b)

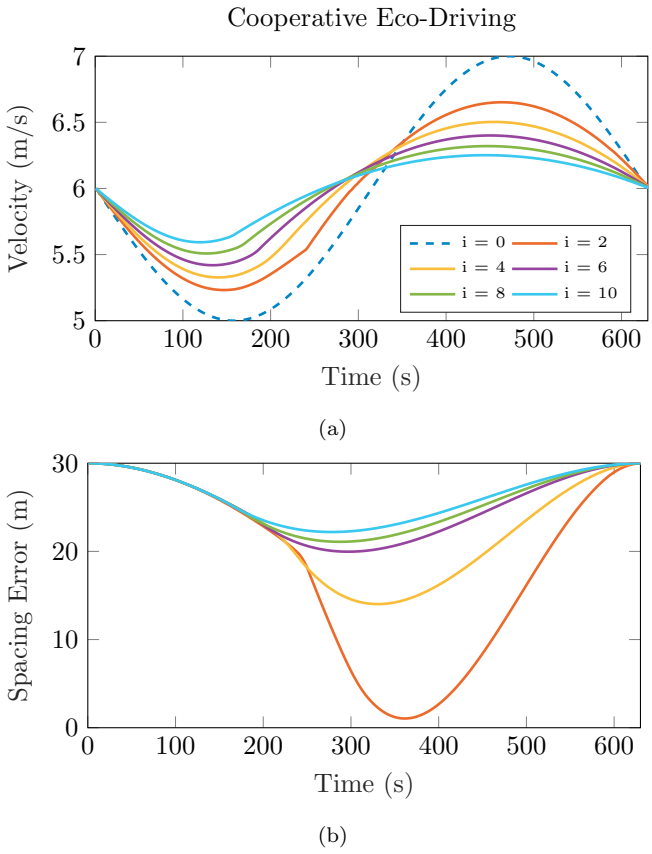

Fig. 6. Velocity profile and spacing error of an eco-driving platoon ($N = 10$) under a sinusoidal perturbation of the leader, with cooperation ($L = 40$ s) (c, d).

Figures 5a–5b show the non-cooperative case where the PV shares only its current acceleration a_{i-1}. At the first time step, the ego vehicle finds its PV decelerating and stopping at a time $t_{stop} = v_{i-1}/|a_{i-1}| = 6/0.01 = 600$ s, which is less than $T_i = 630$ s. This would obstruct the ego vehicle to reach its destination D_i. The controller, therefore based on the condition $t_{stop} < T_i$ chooses (15) as its control input. Since a large negative acceleration a_{i-1} is assumed to persist in the future, the controller tends to overreact to PV acceleration that is likely to change after several seconds. In doing so, the acceleration of each vehicle is larger in magnitude than its PV as we move upstream in the platoon, eventually causing them to come to a stand still. Figure 5a shows the velocity profile of the vehicles in the platoon and Figure 5b the amplification of the spacing error during the beginning of the trip, thus making the platoon string unstable.

In the cooperative case, Figures 6a–6b, the leader $i = 0$ following a known trajectory, now shares its vector of future acceleration over a preview window length $L = 40$ s. The following vehicle $i = 1$, solving its OCP with constant PV acceleration, uses the mean of the acceleration vector $\tilde{a}_{i-1}$ over 40 s rather than instantaneous acceleration a_{i-1}. The mean of the shared acceleration $\tilde{a}_{i-1}$ is now lower in magnitude than the current acceleration a_{i-1}, indicating that the PV is either going to reduce its deceleration or start accelerating in the near future. The condition $t_{stop} < T_i$ now finds the PV to stop at a time after the final time T_i, thereby enabling the controller to use control input (17). Figure 6a shows the velocity profile of the ego vehicles in the platoon. The deceleration of each vehicle is attenuated as we go upstream the platoon, thereby preventing any propagation of spacing error.

5.3 Remarks

The preview window length L is chosen based on a sensitivity analysis for a given trajectory. A too small L could not have any anticipation and a too large L could cause overreaction. The simulations and the theoretical analysis show that the string instability caused under aggressive PV deceleration can be reduced with the help of cooperation.

6. CONCLUSION

The non-cooperative EDOC is energy efficient with a single follower when compared to ACC. However when evaluated in a platoon of several vehicles, it performed worse in terms of energy efficiency and string compactness. These drawbacks were taken as the primary motivation for this study. Cooperation in the form of ability to share intentions over a certain horizon was proposed to improve those drawbacks.The shared intentions over a certain horizon is used in an analytically approach. The proposed cooperative eco-driving was compared using a WLTC High drive cycle with its counterparts, the non-cooperative eco-driving and ACC, in terms of energy efficiency and string compactness. The condition under

which string instability occurs was also investigated by a specific case study.

The results suggested that cooperation has a potential for improvement in platoon energy efficiency and string stability when compared to the non-cooperative eco-driving and ACC. Cooperation was able to mitigate the overreaction of the controller during an aggressive PV deceleration that is likely to change in future.

REFERENCES

Araque, E.S., Colin, G., Cloarec, G.M., Ketfi-Cherif, A., and Chamaillard, Y. (2018). Energy analysis of eco-driving maneuvers on electric vehicles. IFAC-PapersOnLine, 51(31), 195 – 200. doi: https://doi.org/10.1016/j.ifacol.2018.10.036. 5th IFAC Conference on Engine and Powertrain Control, Simulation and Modeling E-COSM 2018.

Dib, W., Serrao, L., and Sciarretta, A. (2011). Optimal control to minimize trip time and energy consumption in electric vehicles. In 2011 IEEE Vehicle Power and Propulsion Conference, 1–8. doi: 10.1109/VPPC.2011.6043133.

Dollar, R., Sciarretta, A., and Vahidi, A. (2020). Information and collaboration levels in vehicular strings: A comparative study. IFAC World Congress 2020.

Dunbar, W.B. and Murray, R.M. (2006). Distributed receding horizon control for multi-vehicle formation stabilization. Automatica, 42(4), 549–558. doi: https://doi.org/10.1016/j.automatica.2005.12.008.

Han, J., Sciarretta, A., Ojeda, L.L., De Nunzio, G., and Thibault, L. (2018). Safe- and eco-driving control for connected and automated electric vehicles using analytical state-constrained optimal solution. IEEE Transactions on Intelligent Vehicles, 3(2), 163–172. doi: 10.1109/TIV.2018.2804162.

Maamria, D., Gillet, K., Colin, G., Chamaillard, Y., and Nouillant, C. (2016). Which methodology is more appropriate to solve eco-driving optimal control problem for conventional vehicles? In 2016 IEEE Conference on Control Applications (CCA), 1262–1267. doi:10.1109/CCA.2016.7587980.

Mahler, G. and Vahidi, A. (2014). An optimal velocity-planning scheme for vehicle energy efficiency through probabilistic prediction of traffic-signal timing. IEEE Transactions on Intelligent Transportation Systems, 15(6), 2516–2523. doi:10.1109/TITS.2014.2319306.

Naus, G.J., Vugts, R.P., Ploeg, J., van De Molengraft, M.J., and Steinbuch, M. (2010). String-stable cacc design and experimental validation: A frequency-domain approach. IEEE Transactions on vehicular technology, 59(9), 4268–4279.

Peppard, L. (1974). String stability of relative-motion pid vehicle control systems. IEEE Transactions on Automatic Control, 19(5), 579–581. doi:10.1109/TAC.1974.1100652. URL https://doi.org/10.1109/TAC.1974.1100652. Cited By 113.

Qi, X., Wang, P., Wu, G., Boriboonsomsin, K., and Barth, M.J. (2017). Energy and mobility benefits from connected ecodriving for electric vehicles. In 2017 IEEE 20th International Conference on Intelligent Transportation Systems (ITSC), 1–6. doi: 10.1109/ITSC.2017.8317744.

Rajamani, R. and Chunyu Zhu (1999). Semi-autonomous adaptive cruise control systems. In Proceedings of the 1999 American Control Conference (Cat. No. 99CH36251), volume 2, 1491–1495 vol.2. doi: 10.1109/ACC.1999.783618.

Sciarretta, A. and Vahidi, A. (2020). Energy-Efficient Driving of Road Vehicles. Springer.

Seiler, P., Pant, A., and Hedrick, K. (2004). Disturbance propagation in vehicle strings. IEEE Transactions on Automatic Control, 49(10), 1835–1842. doi: 10.1109/TAC.2004.835586.

Shaw, E. and Hedrick, J.K. (2007). String stability analysis for heterogeneous vehicle strings. In 2007 American Control Conference, 3118–3125. doi: 10.1109/ACC.2007.4282789.

Sheikholeslam, S. and Desoer, C.A. (1990). Longitudinal control of a platoon of vehicles. In 1990 American Control Conference, 291–296. doi: 10.23919/ACC.1990.4790743.

Shen, D., Karbowski, D., and Rousseau, A. (2020). A minimum principle-based algorithm for energy-efficient eco-driving of electric vehicles in various traffic and road conditions. IEEE Transactions on Intelligent Vehicles, 5(4). doi:10.1109/TIV.2020.3011055.

Swaroop, D. and Hedrick, J.K. (1996). String stability of interconnected systems. IEEE Transactions on Automatic Control, 41(3), 349–357. doi: 10.1109/9.486636.

Swaroop, D. and Hedrick, J.K. (1999). Constant Spacing Strategies for Platooning in Automated Highway Systems. Journal of Dynamic Systems, Measurement, and Control, 121(3), 462–470. doi:10.1115/1.2802497. URL https://doi.org/10.1115/1.2802497.

Wang, M., Daamen, W., Hoogendoorn, S.P., and van Arem, B. (2014). Rolling horizon control framework for driver assistance systems. part i: Mathematical formulation and non-cooperative systems. Transportation Research Part C: Emerging Technologies, 40, 271–289. doi:https://doi.org/10.1016/j.trc.2013.11.023.

Xiao, L. and Gao, F. (2011). Practical string stability of platoon of adaptive cruise control vehicles. IEEE Transactions on intelligent transportation systems, 12(4), 1184–1194.

Yanakiev, D. and Kanellakopoulos, I. (1998). Nonlinear spacing policies for automated heavy-duty vehicles. IEEE Transactions on Vehicular Technology, 47(4), 1365–1377. doi:10.1109/25.728529.